

# Geometrically-Shaped Multi-Dimensional Modulation Formats in Coherent Optical Transmission Systems

Bin Chen, *Senior Member, IEEE*, Yi Lei, *Member, IEEE*, Gabriele Liga, *Member, IEEE*, Zhiwei Liang, Wei Ling, Xuwei Xue, *Member, IEEE*, and Alex Alvarado, *Senior Member, IEEE*

**Abstract**—Shaping modulation formats in multi-dimensional (MD) space is an effective approach to harvest spectral efficiency gains in both the additive white Gaussian noise (AWGN) channel and the optical fiber channel. In the first part of this paper, existing MD geometrically-shaped modulations for fiber optical communications are reviewed. It is shown that large gains can be obtained by exploiting correlation in the dimensions or/and by increasing the cardinality of the modulation format. Practical limitations and challenges are also discussed together with efficient solutions. In the second part, we extend the recently proposed four-dimensional (4D) modulation format family based on the constraint of orthant-symmetry to high spectrum efficiencies up to 10 bit/4D-sym by maximizing generalized mutual information for AWGN channel. Reach increases of up to 25% for a multi-span optical fiber transmission system are reported. Lastly, with the help of a recently introduced nonlinear interference (NLI) model, an optimization for designing nonlinear-tolerant 4D modulation formats is introduced for a single-span optical fiber system. Simulation results show that the proposed NLI model-based 4D modulation format could increase the effective SNRs by 0.25 dB with respect to the AWGN channel-optimal 4D modulation format.

**Index Terms**—Achievable information rates, generalized mutual information, multidimensional modulation format, geometric shaping, nonlinearities, optical fiber communication.

## I. INTRODUCTION

Currently, one of the main challenges in optical fiber transmission systems is to ensure that the available capacity within the deployed systems is efficiently utilized. A key technique to achieve this is to combine forward error correction (FEC) with nonbinary modulation formats, which is known as coded modulation (CM) [2]. For a robust transmission system, a trade-

off between data rate, noise tolerance, demapping-decoding computational complexity has to be made when optimizing constellations for a given transmission distance. 400G (and emerging 800G) optical CM transceivers use polarization-multiplexed (PM) two-dimensional (2D) constellations such as 16-ary quadrature amplitude modulation (QAM) and 64QAM, however, other alternatives exist.

Signal shaping has recently been widely investigated in optical fiber communications to improve spectral efficiency (SE), and is currently implemented in commercial products via probabilistic shaping (PS) [3] and geometric shaping (GS) [4]. Both PS and GS are often used to mimic a Gaussian distribution on the symbols by either changing the probability or the position of each constellation point compared to conventional rectangular structures (i.e., QAM formats). Both techniques have distinct advantages and disadvantages. PS has been shown to offer a near-optimal linear shaping gain and a greater flexibility than GS in general [5, Sec. 4.2], [6]. In addition, by applying PS to a standard QAM constellation, the optimum Gray-labeling can easily be employed. However, PS requires an external distribution matcher (DM) with an efficient implementation and this drawback of PS can limit its shaping gain. GS only requires straightforward modifications of the mapper and demapper, which can be easily coupled with FEC and designed for different impairments (e.g., fibre nonlinearity [7] and laser phase noise [8]). However, the irregular constellation points of GS requires a finer digital-to-analog converter (DAC) and analog-to-digital converter (ADC) precision, and also increases the computational complexity of the demapper. Furthermore, in practical optical fiber system, both PS and GS suffer from rate loss due to the nonlinear effects of the fiber and practical implementation penalty. Research is therefore now dedicated to find improved PS, GS and hybrid PS/GS architectures.

The standard approach in optical fiber systems consists in encoding data independently over each polarization channel using the same 2D modulation format, leading to polarization-multiplexed 2D (PM-2D) formats. For 2D constellations, GS optimizations were already proposed in the 70's in the communication theory literature [9]–[11]. These optimizations were more recently revisited in the context of optical fiber transmission in [12]–[15]. A smaller but still significant amount of work was also performed on constellation design in optical fiber channel with nonlinearities [7], [16]–[20] and laser phase noise [8], [21], [22]. By using 2D GS formats, a record

The work of B. Chen and Y. Lei are supported by the National Natural Science Foundation of China (No. 62171175, 62001151 and 62101065), by the Fundamental Research Funds for the Central Universities (No. JZ2022HGTTB0262). The work of G. Liga is funded by the EuroTechPostdoc programme and the European Research Council under the European Union's Horizon 2020 research and innovation programme (No. 754462). The work of A. Alvarado is supported by the Netherlands Organisation for Scientific Research (NWO) via the VIDI Grant ICONIC (project number 15685). Parts of this paper have been presented at the *Optical Fiber Communication Conference and Exhibition (OFC)*, San Diego, California, USA, 2022 [1].

B. Chen, Y. Lei, Z. Liang and W. Ling are with the School of Computer Science and Information Engineering, Hefei University of Technology, Hefei, China (e-mails: {bin.chen,leiyi}@hfut.edu.cn).

G. Liga and A. Alvarado are with the Department of Electrical Engineering, Eindhoven University of Technology, Eindhoven, The Netherlands (e-mails: {g.liga,a.alvarado}@tue.nl).

X. Xue is with State Key Laboratory of Information Photonics and Optical Communications, Beijing University of Posts and Telecommunications, Beijing, China (e-mail: x.xue@bupt.edu.cn).

TABLE I  
PUBLISHED GAINS OBTAINED BY GEOMETRIC SHAPING IN OPTICAL FIBER COMMUNICATION SYSTEMS: 2D → 4D → 8D → MD.<sup>1</sup>

Modulation	SE	Channel	Baseline	Performance metric	Gain	Description
<b>2D-GS</b>						
GS-16 [14]	4 bit/2D-sym	AWGN	16QAM	MI/GMI	SNR: 0.1–0.2 dB	Optimize for multiple SNRs
GS-32 [13]	5 bit/2D-sym	AWGN/Experiments	32QAM	GMI	SNR: 0.5 dB	SNR=11 dB
GS-64 [15]	6 bit/2D-sym	AWGN/SSFM	64QAM	MI/GMI	SNR: 0.5–0.6 dB	250 km reach ↑ (+12%)
GS-64 [24]	6 bit/2D-sym	Experiments	64QAM	GMI	SNR: 0.5 dB	74.38 Tbit/s in C+L band
GS-128 [18]	7 bit/2D-sym	Experiments	128QAM	BER	SNR: 1–1.2 dB	800 Gb/s, 1 Tb/s
GS-256 [14], [19], [27]	8 bit/2D-sym	AWGN/SSFM	256QAM	MI/GMI	SNR: 0.8 dB	10%–17% reach ↑
IPM-256 [12]	8 bit/2D-sym	Experiments	256QAM	MI	SNR: 0.88 dB	BICM-ID, 800 km (single channel)
GS-1024 [27]	10 bit/2D-sym	AWGN	1024QAM	GMI	SNR: 1 dB	26% reach ↑
GS-64/256/1024 [23]	6–10 bit/2D-sym	Experiments	64/256/1024QAM	GMI	SNR: 0.5–1 dB	18% throughput ↑, 178 Tbit/s in S+C+L band
GS2D/GSNL2D [28]	3–13 bit/2D-sym	AWGN/SSFM	QAM	GMI	SNR: close to 1.53 dB	Optimize for multiple SNR
<b>4D-GS</b>						
PS-QPSK [29], [30]	3 bit/4D-sym	AWGN	PM-QPSK	BER	SNR: 0.97 dB	at BER of $10^{-3}$ , SE: 25% ↓ w.r.t QPSK
8PolSK-QPSK [31]	5 bit/4D-sym	Experiments	PM-8QAM	BER	SNR: 0.5 dB	34% reach ↑, 3800 km
64SP-12QAM [32]	7 bit/4D-sym	Experiments	PM-8QAM	BER	SNR: 0.3 dB	8% reach ↑ (3 channels)
4D2A8PSK [33]	5–7 bit/4D-sym	SSFM	PM-8QAM/32SP-QAM	GMI	SNR: 0.6–2.2 dB	4D constant-modulus, DM link
4D-64PRS [34], [35]	6 bit/4D-sym	AWGN	PM-8QAM	GMI	SNR: 0.7–0.9 dB	4D constant-modulus, DM link
4D-OS128 [36]	7 bit/4D-sym	SSFM/Experiments	128SP-QAM	GMI	SNR: 0.65 dB	16% reach ↑, 11700 km (11 channels)
4D-GSS [37], [38]	8 bit/4D-sym	SSFM	PM-16QAM	MI/GMI	SNR: 0.23–0.27 dB	15% reach ↑, 9000 km (11 channels)
4D-512-Hurwitz [39]	9 bit/4D-sym	AWGN/Experiments	PM-16QAM	MI/GMI	SNR: 0.8 dB	3% reach ↑, single span 160 km (single channel)
$C_{64/128/256/512}^*$ [40]	6–9 bit/4D-sym	SSFM	PM- $M$ QAM/4D-OS128	MI	SNR: 0.2–0.7 dB	Two-stage demodulation, 400G over 120 km
GS4D-4096 [28]	12 bit/4D-sym	AWGN/SSFM	PM-64QAM	GMI	SNR: 0.5–0.8 dB	4%–13% reach ↑ (single channel)
<b>8D-GS</b>						
X-constellation [41]	4 bit/8D-sym	AWGN	PM-BPSK	BER	SNR: 0.53 dB	at BER of $3.5 \times 10^{-2}$
		Experiments		Q-factor	Q-factor: 2 dB	DM link, 5000 km
PB-5b8D, PA-7b8D [42]	5 bit/8D-sym	SSFM	PM-BPSK	Q-factor	Q-factor: 0.1 dB	SE: 25% ↑ w.r.t BPSK
	7 bit/8D-sym	SSFM	PM-QPSK	Q-factor	Q-factor: 0.8 dB	SE: 12.5% ↓ w.r.t QPSK
PB-PS-QPSK [43]	6 bit/8D-sym	SSFM	PS-QPSK	MI	Rate: 1.5 Gb/s	DM link, 10000 km, 35 GbD
8b-8D-sphere [44]	8 bit/8D-sym	SSFM	PM-QPSK	BER	SNR: 0.2–1 dB	at BER of $10^{-2}$ and $10^{-3}$
8D-PRS2048 [45], [46]	11 bit/8D-sym	AWGN+SSFM	PM-8QAM/4D2A8PSK	GMI	SNR: 0.25–0.7 dB	5%–15% reach ↑
		Experiments				EDFA (11 channels)
<b>MD-GS</b>						
12D [47]	12 bit/12D-sym	AWGN	PM-QPSK	BER	SNR: 1.2 dB	at BER of $10^{-4}$
		Experiments		MI	Reach: 8%–15%	MCF, 10000 km (13 channels)
16D [48]	8 bit/16D-sym	Experiments	PM-BPSK	BER	SNR: 2.5 dB	55% reach ↑, MCF, 14000 km (single channel)
24D [49]–[51]	12 bit/24D-sym	Experiments	PM-BPSK	BER	SNR: 2–3 dB	15% reach ↑, 25980 km (single channel)
Voronoi-based MD [52]	24 bit/24D-sym	AWGN/SSFM	PM- $M$ QAM	MI/SER/BER	SNR: 2–3 dB	38% reach ↑, at BER of $2.26 \times 10^{-4}$

SSFM: split-step Fourier method; MCF: multi-core fiber; DM: dispersion-managed; BICM-ID: bit interleaved coded modulation with iterative decoding; ↑: increase; ↓: decrease.

transmission throughput of 178.08 Tbit/s over 40 km and a record capacity transmission of 74 Tbit/s over 6300 km were reported in [23] and [24], respectively. These 2D GS formats are listed in the first part of Table I, which is a broad, but nonexhaustive overview of existing GS works for optical communication systems.

Even though 2D geometric shaping has been shown to increase the achievable information rates (AIRs) in optical fiber systems, these modulations with a finite number of constellation points perform suboptimally in terms of AIR when compared to probabilistically-shaped QAM in the AWGN channel [5, Sec. 4.2], [6]. For both the AWGN and the optical fiber channel, higher shaping gains or/and coding gains are to be expected from modulation formats with a higher number of dimensions [25], [26]. Thus, the design of MD modulation formats has been considered as an effective approach to harvest performance gains in optical communications. These formats include for example 4D, 8D, 12D, 16D, etc., as shown in Table I.

Most of the so-called MD modulation formats in the early literature are in fact only optimized in each complex dimension independently. In this sense, they are not *true* MD modulation formats. This is the case of PM-2D formats, where two identical constellations are transmitted independently over

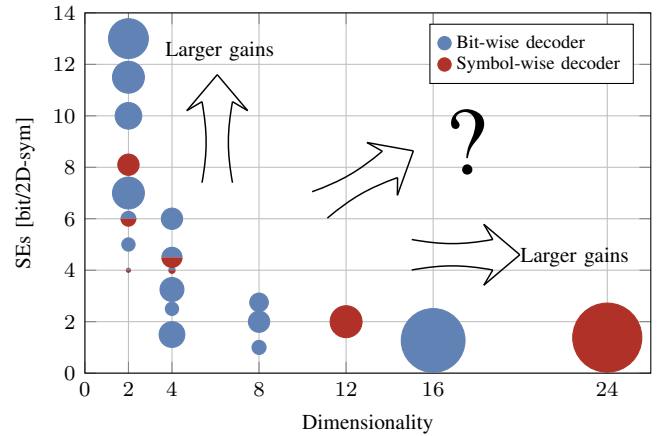


Fig. 1. Illustration of approximate gains of MD geometrically-shaped modulation formats vs. SEs dimensionality. Radii of the markers are proportional to the corresponding SNR gains in Table I with respect to conventional QAM.

two orthogonal polarizations. A true MD format is not in general generated as Cartesian products of a component 1D or 2D constellation. One way to generate MD modulation formats with dependency between dimensions is applying Ungerboeck's set-partitioning (SP) scheme [2], which maps binary bits onto multiple consecutive 2D symbols in a selected subset to generate a MD symbol. For example, in four-dimensional (4D) space, set-partitioning PM-16QAM has been investigated to achieve fine granularity by mapping 5–7 bits onto two consecutive QAM symbols. These formats are known as 32-ary SP 16QAM (32SP-QAM) [53], [54], 64-ary SP 16QAM (64SP-QAM) [32] and 128-ary SP 16QAM (128SP-

<sup>1</sup>All the reported results in Table I are compared with the baselines at the same SE and under the same FEC overhead assumption, except PS-QPSK in [29], [30], 8PolSK-QPSK in [31], 4D-512-Hurwitz in [39], and the 8D formats in [42], which however do make a fair comparison by modifying symbol rate or FEC overhead.

QAM) [55]–[57]. 4D set-partitioned formats based on the  $D_4$  lattice have also been investigated by using multilevel coding and multi-stage decoding [39].

One of the main advantages of performing shaping in MD space is that it can also be used to mitigate the nonlinear effects in the optical fiber channel. This insight motivates the search for modulation formats in a higher dimensional space that are tolerant to linear noise and/or nonlinear interference (NLI) [58]. Intuitively, waveforms with less intensity variation generate lower NLI. Therefore, 4D constant modulus constellations were first proposed to achieve better nonlinearity tolerance performance compared to multi-modulus ones [29]–[31], [33], [34], [59], [60]. For example, polarization switched-QPSK (PS-QPSK) [29], [30] maps 3 bits onto two consecutive QPSK symbols, while 4D2A8PSK [33] maps 5–7 bits onto two consecutive 8PSK symbols in both X- and Y-polarization. 4D-64PRS [34] is obtained by maximizing generalized mutual information (GMI) under the constraint of 4D constant modulus and was transmitted over 11,700 km in a laboratory experiment with standard single-mode fiber (SSMF) [35]. More generally, an MD modulation format can “shape out” the partial NLI at the expense of losing some degrees of freedom [58]. Furthermore, increasing the dimensionality provides flexibility to optimize the constellation power efficiency and introduces specific correlations between different dimensions that can further reduce the generation of nonlinear effects during signal propagation.

MD modulation formats in 8D [41], 12D [47], 16D [48] and 24D [49]–[51] have been proposed by adding proper constraints in the optimization to mitigate modulation-dependent NLI interaction and to extend the transmission reach. For example, the eight dimensions were obtained in [61] by combining two polarizations with two frequencies and in [41], [44] by using two consecutive time slots. In [42], [43], [45], [46], 8D modulation formats in two consecutive time slots were designed to further mitigate fiber nonlinear impairments using the polarization-balancing or polarization-alternating concept. 24D modulation formats in optical systems were also demonstrated based on sphere cutting of lattices and block codes (as inner codes) in [49], [51] and 15% reach increase was shown over BPSK in [50]. In [47], a 12D modulation format was demonstrated across three linearly coupled spatial modes of a multicore fiber showing improved performance over PM-QPSK. To pack the constellation points more efficient, ultra-large Voronoi constellations with up to  $10^{28}$  MD points and larger SE were recently demonstrated in [52] to show significant bit error rate (BER) and symbol error rate (SER) gains over QAM.

The approximated gains in terms of SNR for MD geometrically-shaped modulation in Table I are shown in Fig. 1 for different dimensionalities and SEs. Fig. 1 shows that (i) large constellation sizes can potentially achieve large gains, (ii) high dimensionalities can potentially achieve large gains, (iii) research has mainly focused on the optimization of constellations either in a low-dimensional space (with high SE), or on high-dimensional constellations (but with relatively low SE). As shown in Fig. 1, the current challenge is the full optimization of the constellation in a high-dimensional space

with higher SEs to achieve large gains.

The contributions of this paper are three. First, we provide a review of existing multidimensional geometric shaping (MD-GS) works to provide more insights, e.g., limitations and challenges, into the employed MD-GS modulation formats in optical fiber systems. In particular, we also discuss methods for enabling efficient MD-GS performance enhancement and complexity reduction to achieve both linear shaping gains and nonlinearity tolerance. Secondly, in this paper we focus on designing 4D modulation formats for soft-decision (SD) FEC with 20%-25% overhead in bit-interleaved coded modulation (BICM) systems by maximizing the GMI and thus, increasing transmission reach. Simulation comparisons for a set of AWGN-optimized 4D formats with SEs of 5–10 bits/4D-sym, which outperform PM-MQAM and the previously known 4D formats, are presented in a multi-span optical fiber communication system. Finally, to design nonlinear-tolerant modulation formats in optical fiber systems, an optimization of dual-polarization (DP) modulation based on the 4D NLI model [62] is performed to mitigate NLI in a single-span transmission scenario.

The remainder of this paper is structured as follows. In Sec. II, we present the system model adopted for our constellation design and introduce the performance metrics for the MD coded modulation system under consideration. In Sec. III, we discuss general aspects of MD geometric shaping. In Sec. IV, we present the methods for enabling efficient multi-dimensional modulation optimization and its implementation. The simulation results of optical fiber transmission for multi-span system and single-span system are further presented in Sec. V and Sec. VI, respectively. Finally, the paper is concluded in Sec. VII.

*Notations:* Bold symbols denote either row vectors (lower case) or random vectors (upper case). The elements of a vector  $\mathbf{x}$  are denoted by  $x_i$ , and the element at row  $i$ , column  $j$  of a matrix  $\underline{\mathbf{x}}$  are denoted by  $x_{i,j}$ . Expectation denoted by  $\mathbb{E}[\cdot]$  and the squared Euclidean of  $N/2$ -dimensional complex vector is defined as  $\|\mathbf{X}\|^2 = |X_1|^2 + |X_2|^2 + \dots + |X_N|^2$ . The set is denoted by  $\mathcal{A}$  and the Cartesian product between sets is denoted by  $\mathcal{A} \times \mathcal{A}$ .

## II. SYSTEM MODEL AND PERFORMANCE METRICS

### A. System Model with Multi-Dimensional Modulation Format

In this paper, we consider the most popular bit-wise CM scheme for optical communication systems, i.e., a BICM system shown in Fig. 2. The optical channel with memory can be modeled by a conditional probability density function (PDF)  $p_{\mathbf{Y}|\mathbf{X}}$  with input sequence  $\underline{\mathbf{X}}$  and output sequence  $\underline{\mathbf{Y}}$ . The transmitted symbols  $\mathbf{X}$  and received symbols  $\mathbf{Y}$  in  $\underline{\mathbf{X}}$  and  $\underline{\mathbf{Y}}$  are assumed to be MD symbols with  $N/2$  complex dimensions (or equivalently, with  $N$  real dimensions). We use  $k \in \{1, 2, \dots, m\}$  to indicate the bit position in a length- $m$  binary sequence,  $j \in \{1, 2, \dots, N/2\}$  to indicate the complex dimension and  $l \in \{1, 2, \dots, n_s\}$  to indicate the time instant.

At the transmitter, the encoders generate coded bits  $\underline{\mathbf{c}} = [c_1; c_2; \dots; c_m]$ , where  $\mathbf{c}_k = [c_{k,1}, c_{k,2}, \dots, c_{k,n_s}]$ ,  $k = 1, 2, \dots, m$  is the bit position and  $n_s$  is the block length in

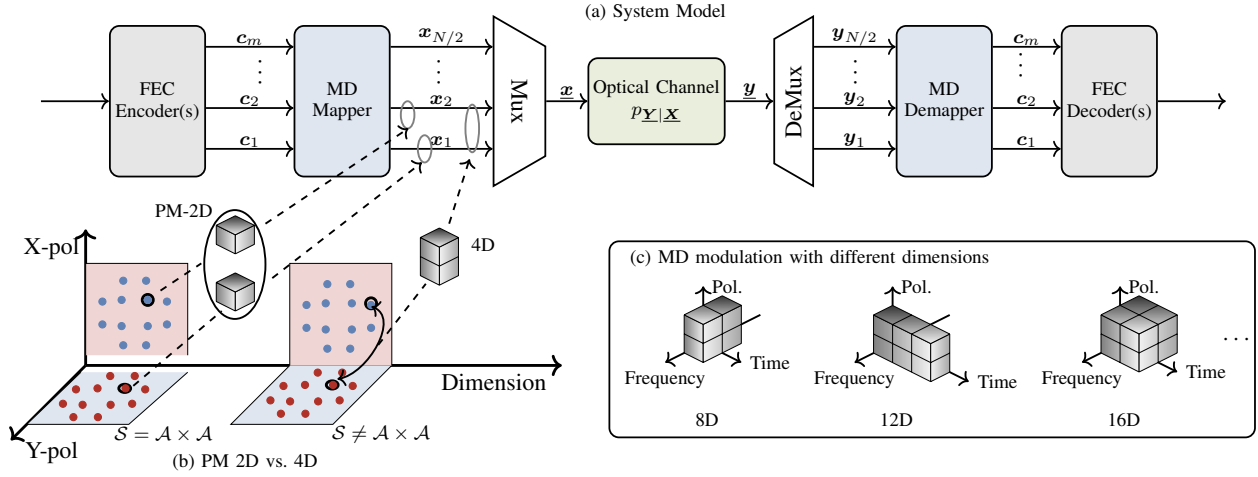


Fig. 2. Block diagram of CM transceiver employing MD modulation format under consideration. The transmitter consists of a binary FEC encoder followed by a MD mapper. The MD mapper can either separately and jointly generate the MD symbols  $\underline{x}$ . Each cube denote a two-dimensional real signal space, which is most intuitively viewed as the complex-valued symbol.

symbols. The coded bits are grouped into a length- $m$  binary sequence and are mapped to the MD symbols

$$\underline{x} = [\underline{x}_1; \underline{x}_2; \dots; \underline{x}_{N/2}] = \begin{bmatrix} x_{1,1} & x_{1,2} & \dots & x_{1,n_s} \\ \vdots & \vdots & \ddots & \vdots \\ x_{N/2,1} & x_{N/2,2} & \dots & x_{N/2,n_s} \end{bmatrix},$$

where the  $l$ th MD symbol  $[x_{1,l}; x_{2,l}; \dots; x_{N/2,l}]$  in each column is drawn from a discrete constellation  $\mathcal{S} \triangleq \{\mathbf{s}_1; \mathbf{s}_2; \dots; \mathbf{s}_M\}$ . Throughout this paper the  $i$ th  $N$ -dimensional constellation point is denoted by  $N/2$ -dimensional complex symbol as  $\mathbf{s}_i = [s_{i,1}, s_{i,2}, \dots, s_{i,N/2}] \in \mathbb{C}^{N/2}$  with  $i = 1, 2, \dots, M$ . The  $i$ th constellation point  $\mathbf{s}_i$  is labeled by a length- $m$  binary sequence  $\mathbf{b}_i = [b_{i,1}, b_{i,2}, \dots, b_{i,m}] \in \{0, 1\}^m$  from a binary labeling set  $\mathcal{B} \triangleq \{\mathbf{b}_1, \mathbf{b}_2, \dots, \mathbf{b}_M\}$  using a one-to-one mapping  $\mathbf{b}_i \rightarrow \mathbf{s}_i$ .

As shown in Fig. 2 (a), the general structure of MD mapper can be used to generate arbitrary multi-dimensional modulation formats at transmitter. There are multiple ways to map the MD modulation to generate the optical signal. The two most popular cases of 4D modulation in fiber optical communications are shown in Fig. 2 (b) as examples, which correspond to coherent optical communications using two polarizations of the light (each polarization includes two real dimensions, i.e., in-phase  $I$  and quadrature  $Q$ ). Each cube denote a two-dimensional real signal space, this naturally results in 4D modulation format as two cubes in Fig. 2 (b). In this case, the 4D modulation  $\mathcal{S}$  can be independently and separately transmitted in each complex dimension (polarization) as PM-2D, i.e., a single 2D modulation  $\mathcal{A}$  is used to independently map information over two orthogonal polarization modes of the optical signal shown as two independent cubes. If  $\mathcal{S} \neq \mathcal{A} \times \mathcal{A}$ , the 4D modulation  $\mathcal{S}$  in  $2 \times 2$ D spaces are neither identically or independently distributed, and thus, are jointly transmitted over 4D spaces shown as two bonded cubes with dependency.

In Fig. 2 (a) and (b), we consider 4D modulation formats using  $N$ -dimensional space and group into  $N/4$  wavelength to form a wavelength division multiplexing (WDM) signal over the optical fiber channel as an example. Actually, the

4D symbols (two cubes) can be also transmitted over other  $N/4$  different dimensions, e.g., time slot, spatial mode, etc. These degrees of freedom (wavelength, time slot and spatial mode) can be used to increase the number of dimensions, it can also extend 4D modulation formats to 8D, 12D, 16D and even higher dimensional modulation formats, which are shown as multiple cubes in Fig. 2 (c).

### B. Performance Metrics for BICM System

Due to its simplicity and flexibility, BICM with SD-FEC is usually considered as an attractive option for optical fiber communication systems [63], and hence, the use of the information-theoretical performance metric GMI is preferred for coded modulation design [64]. Since the actual channel statistics are unknown, the actual conditional distribution  $p_{\mathbf{Y}|\mathbf{X}}$  must be approximated by a suboptimal mismatched channel law  $q_{\mathbf{Y}|\mathbf{X}}$  under the assumption of memoryless and also using bit-metric decoder [64]. The GMI is the most popular AIR for a BICM system and can be expressed as

$$G(\mathcal{S}, \mathcal{B}, q_{\mathbf{Y}|\mathbf{X}}) = \sum_{k=1}^m I(B_k; \mathbf{Y}), \quad (1)$$

where  $\mathbf{B} = [B_1, B_2, \dots, B_m]$  is a random vector representing the transmitted bits  $\mathbf{c}_l = [c_{1,l}, c_{2,l}, \dots, c_{m,l}]$  at time instant  $l$ , which are mapped to the corresponding symbol  $\mathbf{X}_l$ . In Eq. (1),  $I(B_k; \mathbf{Y})$  is the mutual information (MI) between the bits and the symbols, and the notation  $G(\mathcal{S}, \mathcal{B}, q_{\mathbf{Y}|\mathbf{X}})$  emphasizes the dependency of the GMI on the constellation, binary labeling, and mismatched channel law. Furthermore, for any  $N$ -dimensional channel law, Eq. (1) can be expressed as [64, Eqs. (15)–(18)]

$$\begin{aligned} G(\mathcal{S}, \mathcal{B}, q_{\mathbf{Y}|\mathbf{X}}) &= \sum_{k=1}^m \mathbb{E}_{B_k, \mathbf{Y}} \left[ \log_2 \frac{q_{\mathbf{Y}|B_k}(\mathbf{Y}|B_k)}{q_{\mathbf{Y}}(\mathbf{Y})} \right] \\ &= m + \frac{1}{M} \sum_{k=1}^m \sum_{b \in \{0,1\}} \sum_{i \in \mathcal{I}_k^b} \\ &\int_{\mathbb{C}^{N/2}} q_{\mathbf{Y}|\mathbf{X}}(\mathbf{y}|\mathbf{x}_i) \log_2 \frac{\sum_{p \in \mathcal{I}_k^b} q_{\mathbf{Y}|\mathbf{X}}(\mathbf{y}|\mathbf{x}_p)}{\sum_{p'=1}^M q_{\mathbf{Y}|\mathbf{X}}(\mathbf{y}|\mathbf{x}_{p'})} d\mathbf{y}, \quad (2) \end{aligned}$$

where  $\mathcal{I}_k^b \subset \{1, 2, \dots, M\}$  with  $|\mathcal{I}_k^b| = M/2$  is the set of indices of constellation points whose binary label is  $b \in \{0, 1\}$  at bit position  $k$ .

The GMI can be approximated using Monte-Carlo integration but also via Gauss-Hermite quadrature [64]. The nonlinear optical channel is a channel with memory, and thus, the GMI Eq. (1) can be considered a lower bound on the capacity of the channel [65, Sec. V]. Monte-Carlo integration is better suited for constellations with more dimensions or when the channel law is unknown, while Gauss-Hermite quadrature estimation is better-suited for numerical optimization when the channel is known analytically and it matches a quadrature.

For a discrete uniformly-distributed  $N$ -dimensional modulation, the GMI under Gaussian noise assumption ( $q_{\mathbf{Y}|\mathbf{X}}$  is a circularly symmetric Gaussian PDF with variance  $\sigma_z^2$ ) can be estimated via Gauss-Hermite quadrature estimation as [64, Eq. (45)]

$$\text{GMI} \approx m - \frac{1}{M\pi^{N/2}} \sum_{k=1}^m \sum_{b \in \{0,1\}} \sum_{i \in \mathcal{I}_k^b} \sum_{l_1=1}^J \alpha_{l_1} \sum_{l_2=1}^J \alpha_{l_2} \cdots \sum_{l_N=1}^J \alpha_{l_N} \cdot g_i^G(\boldsymbol{\xi}), \quad (4)$$

with

$$g_i^G(\boldsymbol{\xi}) = \log_2 \frac{\sum_{p=1}^M \exp\left(-\frac{\|\mathbf{d}_{ip}\|^2 + 2\sigma_z \Re\{(\xi_{l_1} + j\xi_{l_2})\mathbf{d}_{ip}\}}{\sigma_z^2}\right)}{\sum_{j \in \mathcal{I}_k^b} \exp\left(-\frac{\|\mathbf{d}_{ij}\|^2 + 2\sigma_z \Re\{(\xi_{l_1} + j\xi_{l_2})\mathbf{d}_{ij}\}}{\sigma_z^2}\right)},$$

where the quadrature nodes  $\xi_l$  and the weights  $\alpha_l$  can be easily found (numerically) for different values of  $J$ .  $\mathbf{d}_{ij} \triangleq \mathbf{s}_i - \mathbf{s}_j$  denotes the difference between two MD symbols and  $\sigma_z^2$  is the noise variance per complex dimension.

In this paper, we use Gauss-Hermite quadrature estimation for modulation optimization with the quadrature nodes and weights for  $J = 10$  in [64, Table III]. For transmission performance evaluation, the Monte-Carlo approximation in [64, Eq. (31)] is used to estimate GMI for the considered modulation formats.

### III. GENERAL ASPECTS OF MD GEOMETRIC SHAPING

#### A. GMI-Based GS Modulation Optimization

As shown in Eqs. (1) and (4), the computation of the GMI requires a joint consideration of the modulation's coordinates and its binary labeling. A GMI-based optimization under a constraint of the transmitted power  $\sigma_x^2$  can be defined as

$$\{\mathcal{S}^*, \mathcal{B}^*\} = \underset{\mathcal{S}, \mathcal{B}: E[\|\mathbf{X}\|^2] \leq \sigma_x^2}{\text{argmax}} G(\mathcal{S}, \mathcal{B}, q_{\mathbf{Y}|\mathbf{X}}), \quad (5)$$

where  $\mathcal{S}^*$  and  $\mathcal{B}^*$  represent the optimal constellation and labeling solution for a given channel conditional PDF  $q_{\mathbf{Y}|\mathbf{X}}$ .

Different optimization methods have been used to solve Eq. (5). Traditional optimizers include for example genetic algorithm [66], pairwise optimization algorithm [13] and particle swarm optimization [20]. In recent years, considering the entire communication system design as an end-to-end reconstruction task have received a lot of attention and the transmitter can be implemented as a trainable GS mapper via a

neural network [16], [17], [19], [27], [67]. A key advantage of the neural network method is that it can be applied to arbitrary channel also considering transceiver hardware impairments, including hardware imperfections and nonlinear optical ones. For more details on end-to-end learning for optical communication systems, we refer the reader to [67, Table I] and references therein.

For MD modulation formats, four main factors have been identified as key factors for improving performance and complexity in the optimization: (i) the SNR range where optimization is performed; (ii) the initial shape for a specific SNR region; (iii) the bit labeling of the initial constellation; (iv) the number of degrees of freedom (DOFs) of the constellation to be designed. These factors are not very important for 1D or 2D modulation optimization, but will become crucial as the dimensionality and cardinality size increase.

#### B. Limitations and Challenges for MD-GS Implementation

The main advantage of GS is that it only relies on the selection of the location of constellation points and the design of the corresponding detector. However, some practical limitations or challenges in realistic CM schemes must be considered that can limit the applicability of GS in optical communication systems. Some drawbacks in GS schemes have been briefly discussed for example in [68, Sec. I]. In this section, we will discuss some limitations and challenges of MD-GS. The focus is mainly on the AWGN channel, however most of these limitations are also applicable to the optical channel.

1) *Nonconvex multi-dimensional optimization problem*: One problem often overlooked when designing MD modulation formats for BICM system is the difficulty of finding locations of the GS constellation points with their labeling for arbitrary channel conditions and arbitrary SEs. It has been shown that the optimization landscape for GMI-based optimization is highly nonconvex and the initialization is an important design parameter, especially for the AWGN channel [27]. Therefore, finding optimum modulation formats with good labeling based on brute force approaches quickly fails as the constellation size grows [69]. It should be noted that none of the existing approaches give guarantees on finding the global optimum. However, the reported results of the optimized constellations do outperform their counterparts (e.g., MQAM) in the considered cases. In order to efficiently solve the nontrivial optimization problem, a fast and accurate GMI computation is crucial. To support an efficient MD-GS via solving the nontrivial optimization problem in Eq. (5), GMI estimation should be accelerated and the search space  $\{\mathcal{S}^*, \mathcal{B}^*\}$  for optimization needs to be reduced.

2) *Hardware limitations*: Another inherent assumption in most of existing GS works is that ideal digital-to-analog converters (DACs) and analog-to-digital converters (ADCs) are included at the transceiver. In order to generate and detect high-order modulation formats, especially for geometrically-shaped modulation formats, DACs and ADCs with a high number of resolution bits are required [70]. For commercial quantizers with 8-bit physical resolution and  $\sim 5$ -6 effective number of bits (ENOB), the use of shaped high-order modulation formats may induce additional penalties due to the

finite resolution of DAC and ADC. It has been estimated that 20% power reduction can be obtained when lowering the resolution from 8 to 4 bits [71]. However, GS in general induces higher peak of the driving signal's amplitude, which results in a larger quantization penalty with low resolution DAC. Depending on the application, it is more meaningful to include finite resolution of DAC and ADC in the analysis and design hardware-friendly MD modulation formats.

3) *Irregular Demapping*: Due to the general infeasibility of Gray mapping for MD modulation formats after GS, the computational complexity of demapping symbols to soft-decision bit metrics, i.e., log-likelihood ratios (LLRs), will be increased. To alleviate the computational complexity of LLR calculation, the well-known max-log approximation is often used and particularly interesting for the AWGN channel. With this approximation, LLRs for bit-wise decoding at any time instant can be computed as follows

$$\Lambda_k \approx \log \frac{\max_{\mathbf{x} \in \mathcal{I}_k^1} q_{Y|X}(\mathbf{y}|\mathbf{x})}{\max_{\mathbf{x} \in \mathcal{I}_k^0} q_{Y|X}(\mathbf{y}|\mathbf{x})}. \quad (6)$$

The max-log approximation therefore eliminates the exponential functions and reduces the number of Euclidean distance (ED) calculations in a maximum likelihood (ML) optimum demapper. For the MD AWGN channel, the max-log LLR values in Eq. (6) are calculated as

$$\Lambda_k \approx \frac{N}{\sigma_z^2} \left( \min_{\mathbf{x} \in \mathcal{I}_k^0} \|\mathbf{y} - \mathbf{x}\|^2 - \min_{\mathbf{x} \in \mathcal{I}_k^1} \|\mathbf{y} - \mathbf{x}\|^2 \right). \quad (7)$$

For each MD received signal, the max-log demapper needs to calculate all  $M = 2^m$  squared EDs in a  $N$ -dimensional space. In the case square QAM or PM-QAM modulation, the max-log approximation results in piece-wise linear relationships between the received symbol and the LLRs in 1D. This means the LLRs in this case can be calculated per real dimension rather than in  $N$  dimensions. This in turn greatly simplifies its implementation, which is partly why the max-log approximation is very popular in practice. For nonsquare QAM or non-Gray-labeled modulation formats, however, this is not the case. For most of MD modulation formats, demapper complexity could be significantly increased due to the larger number of EDs calculation or larger memory requirements for pre-computed look-up table. In order to reduce the computational complexity by avoiding all possible EDs calculation, the MD modulation formats with a regular structure are preferred, e.g., lattice structures, symmetric structures and shell structures.

#### IV. METHODS FOR ENABLING EFFICIENT MD GEOMETRIC SHAPING AND ITS IMPLEMENTATION

In this section, four potential methods of overcoming the limitations discussed in Sec. III-B are shown. The first two methods aim to accelerate the GMI approximation while keeping high accuracy (*Example 1* and *2*). Next, symmetric constraints are added to simplify the optimization and to reduce the hardware penalty (*Example 3*). Finally, performance metrics for assessing modulation-dependent NLI are discussed (*Example 4*).

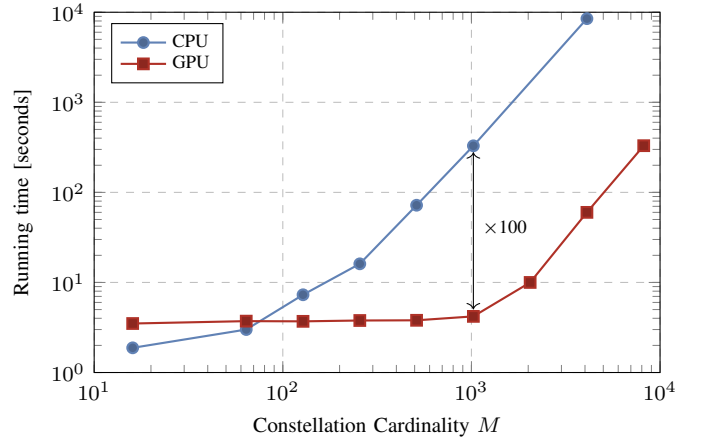


Fig. 3. Comparison of GMI estimation running time between CPU and GPU for 4D modulation formats via Gauss-Hermite quadrature (Eq. (4)). Results were obtained on a workstation with an Intel Core i7-11700 CPU and a NVIDIA GeForce RTX 3090 GPU, respectively.

*Example 1 (GPU-acceleration for GMI estimation)*: It is known that GMI-based optimization of large constellations with high dimensionality (i.e., the top right corner of Fig. 1) is computationally demanding. This has been considered as a challenging issue for such large constellations since the exact MI and GMI estimation requires enumerating all constellation points (*Example 2* will discuss a weighted sampling method to avoid enumerating all the points.). To solve this computation issue, parallel GPU computing can be used to accelerate the computational speed of GMI by parallelizing the quadrature approximation in Eq. (4). Fig. 3 shows a comparison of GMI computation running time between CPU and GPU for 4D modulation formats with different cardinality size  $M = \{16, 64, 128, 256, 512, 1024, 2048, 4096, 8192\}$ . The simulation was obtained with using an Intel Core i7-11700 CPU and an NVIDIA GeForce RTX 3090 GPU via Python. The results shown in Fig. 3 indicate that the GPU-based GMI estimation is at least 100 times faster than the CPU-based when the constellation cardinality size larger than  $10^3$ . Note that the running time of GPU-based GMI estimation also increases due to the parallelization degree limitation of the used GPU when the constellation cardinality is very large. Thus, larger speed-ups are expected when using more powerful GPUs or multi-GPUs architecture. Overall, this acceleration can greatly simplify to make the MD constellation optimization to be possible.  $\triangle$

In the following example, the GMI estimation for very large constellations is particularized to the relevant case of Monte-Carlo integration.

*Example 2 (Low complexity GMI estimation for very large constellations)*: To numerically estimate Eq. (3), the key point is to calculate  $q_Y(\mathbf{y}) = \frac{1}{M} \sum_{\mathbf{x} \in \mathcal{S}} q_{Y|X}(\mathbf{y}|\mathbf{x})$ , which is infeasible when  $M$  is very large. Even though Monte-Carlo techniques can somewhat estimate the GMI faster than the Gauss-Hermite method, they can be very inaccurate when the total number samples are limited, as shown in [5, Example 4.26]. One way is to use a weighted sampling method, called importance sampling, which oversamples from the important region, thus making Monte-Carlo accurate [72].

The intuition behind importance sampling is that only a fraction of all constellation points contribute significantly to the sum in Eq. (3). By following the method in [72, Eqs. (22)–(23)], GMI estimation based on Monte-Carlo method can be simplified but also accurate by choosing a proper important constellation set. For constellation with good structure, e.g., Voronoi constellation with around  $10^{46}$  32-dimensional lattice points, only  $10^5$  random samples for each important subset are needed for accurate GMI estimation.  $\triangle$

The discussed methods in *Example 1* and *Example 2* show that the optimization in Eq. (5) for high-dimensional modulation formats can be made significantly more efficient by accelerating the GMI estimation. However, the search space for large constellations and/or for constellations with high dimensionality is still computationally very demanding due to the large continuous search space. In addition, potentially irregular formats obtained after optimization also impose strict requirements on the generation and detection of the signals, due to the need of high-resolution DACs and ADCs. To solve the multi-parameter optimization challenges of MD-GS and also to achieve a good performance-complexity trade-off, constraints such as constant modulus [33], [34], orthant-symmetry (OS) [36], X-Y symmetry and 4D shells [37], [38] have been proposed to design MD formats. These solutions have shown a small performance loss with respect to the unconstrained optimizations in AWGN channel (or linear region of optical channel), but can achieve even better performance in the nonlinear optical fiber channel.

*Example 3 (Orthant-symmetry constraint):* For an  $N$ -dimensional constellation  $\mathcal{S}$  with  $M = 2^m = |\mathcal{S}|$  points, each point in  $\mathcal{S}$  has four DOFs. Thus, geometrically optimizing a 4D constellation in an unconstrained way results in  $N \cdot 2^m$  DOFs, which quickly becomes challenging as  $N$  and  $m$  increase. To reduce the number of DOF for MD geometric shaping and also to reduce the transceiver requirements, OS constraint has been proposed in [36] to reduce the dimensionality of searching space within the first orthant. Orthant-symmetric labeled constellations can be generated from any first-orthant constellation, where the constellation points are obtained by folding the first-orthant points to the remaining orthants. For a more detailed description of these concepts, we refer the reader to [36]. In addition, a recent work combining OS with X-Y symmetry and 4D shells constraints has been investigated in the context of 400ZR standard [37], [38].

By applying the OS constraint, the optimization problem in Eq. (5) can be simplified as

$$\{\mathcal{S}_1^*, \mathcal{B}_1^*\} = \underset{\mathcal{S}_1, \mathcal{B}_1: E[|X|^2] \leq \sigma_x^2}{\operatorname{argmax}} \{G(\mathcal{S}, \mathcal{B}, q_{Y|X})\} \quad (8)$$

where  $\mathcal{S}_1 \subset \mathcal{R}^+$  and  $\mathcal{B}_1$  denote the first-orthant constellation points and their corresponding labelings. The obtained solution  $\{\mathcal{S}_1^*, \mathcal{B}_1^*\}$  can be used to obtain the complete labeled constellation  $\{\mathcal{S}, \mathcal{B}\}$ . Therefore, the OS constraint can reduce the amount of DOFs by a factor of  $2^N$ .

The insets of Fig. 4 show 2D projections of two AWGN-optimized constellations with  $N = 4$  and  $M = 128$ , where inset (a) is obtained via Eq. (5) (called 4D-GS128), and inset (b) is optimized with an OS constraint by solving Eq. (8)

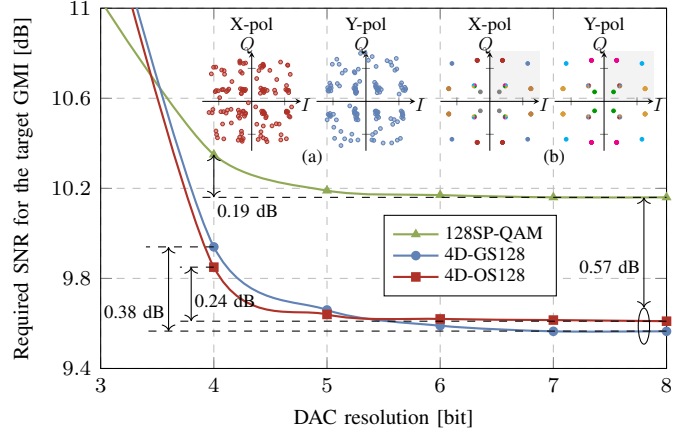


Fig. 4. Required SNR vs. DAC resolutions for three 4D 128-ary modulation formats at GMI of 5.95 bit/4D-sym. Insets: (a) optimized via Eq. (5) as 4D-GS128, (b) optimized via Eq. (8) as 4D-OS128.

(called 4D-OS128). The amount of DOFs is reduced from  $4 \cdot 2^7 = 2^9$  to  $4 \cdot 2^7 / 2^4 = 32$ . As shown in [73], the optimization with OS constraint is much faster to be converged and potentially avoid a suboptimal result with respect to the optimization without OS constraint. In addition, the constellation in Fig. 4 (a) is not well structured, which could lead to a high penalty when using high-speed DAC with limited ENOB. Therefore, adding a proper constraint, e.g. OS, does not only increase optimization speed, but also reduces the DAC/ADC resolution requirements.

In order to compare the impact of finite-resolution DACs, three modulation formats (128SP-QAM, 4D-GS128 and 4D-OS128) are evaluated. At the transmitter, the symbol sequence at 2 samples per symbol was filtered with pulse shaping filter, and then the driving signals are linearly quantized with a variable number of quantization levels for DAC. The effect of the ADCs are not considered in this example. To measure the impairments of limited DAC resolution, we measured the minimum SNR required to achieve the target GMI. The results of the numerical simulations at a symbol rate of 45 GBd over AWGN channel are shown in Fig. 4. It shows the required SNR at GMI of 5.95 bit/4D-sym as function of the DAC resolution for three modulation formats. When comparing the performance at high DAC resolutions, the two 4D shaped modulation formats can provide around a gain of 0.57 dB. We can also observe that decreasing the DAC resolution below four bits results in significantly penalties for all modulation formats. Despite the small gains provided by 4D-GS128 at high DAC resolutions, when the DAC resolution is reduced to 4, the performance of 4D-GS128 (0.38 dB penalty) degrades more rapidly than 4D-OS128 (0.24 dB penalty) and 128SP-QAM (0.19 dB penalty) due to the larger quantization distortion for the neighboring points.  $\triangle$

*Example 4 (Performance metrics for nonlinearity-tolerant 4D modulation):* Fig. 5 shows NLI-related performance metrics versus iteration number in the optimization process for two sets of 4D modulation formats: AWGN-optimized (blue lines) and NLI-optimized (red lines). AWGN-optimized modulation formats are obtained by maximizing GMI for a fixed SNR, while NLI-optimized formats are obtained by maximizing

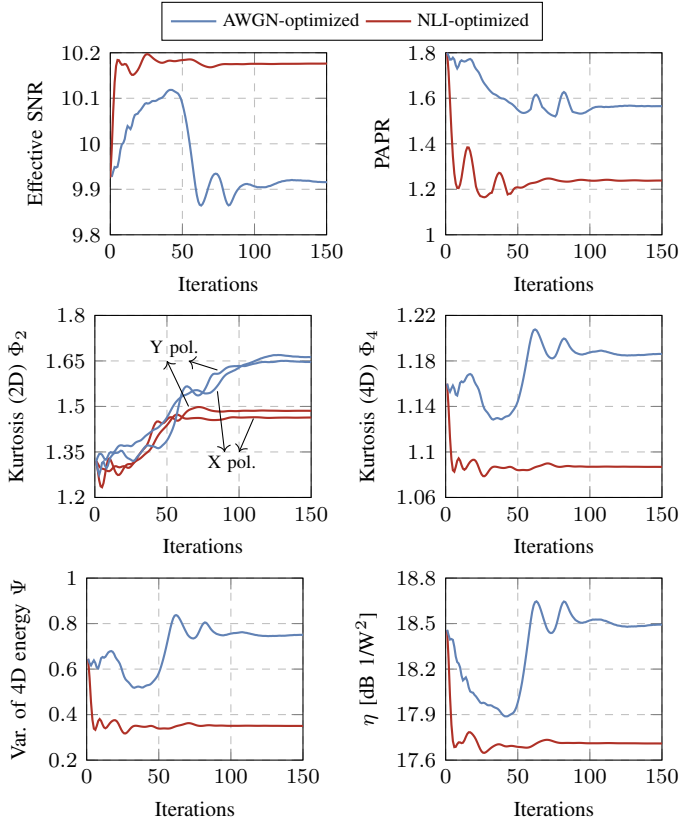


Fig. 5. NLI-related performance metrics vs. the 4D modulation optimization process for optical fiber simulations of single channel with symbol rate of 45 GBaud over single span of 234 km single-mode fiber (see Sec. VI for details of optimization). The 4D symbol sequences are normalized to  $E[\|\mathbf{X}\|^2] = 2$  to compute the performance metrics.

GMI with considering the NLI power to trade-off between shaping and nonlinearity in nonlinear channel. To evaluate the NLI effect of the optimized modulation formats in the optical channel, we consider a dual-polarized, single channel waveform over a 234 km single span SSMF. More details about the nonlinearity-tolerant 4D modulation optimization are given in Sec. VI. By treating the modulation-dependent NLI as Gaussian noise, the change in modulation by moving the 4D symbols during the optimization can be reflected in effective SNR as shown in Fig. 5.

In Fig. 5, the nonlinear tolerance related performance metrics for showing variations of symbol energies, i.e., peak-to-average power ratio (PAPR), kurtosis (here, we use  $\Phi_2$  and  $\Phi_4$  to denote the kurtosis of 2D symbols and 4D symbols, respectively), the variance of the transmitted 4D symbols' energy  $\Psi$  and the NLI power coefficient  $\eta$  (see [74, Eq. (1)]) are also shown for each optimized 4D formats during the iterative optimization.<sup>2</sup>

By comparing the optimization traces between the AWGN-optimized (blue lines) and NLI-optimized formats (red lines), we can observe that an NLI-tolerant 4D modulation format

<sup>2</sup>Note that the variance of the transmitted 4D symbols' energy is the deviation of the signal energy from the mean value and is also determined by the kurtosis of the 4D transmitted symbol as  $\Psi = \mathbb{E}[\|\mathbf{X}\|^2](\Phi_4 - 1)$  [75, Eq. (48)]. Similar metrics with considering sliding window were defined in [75], [76] to evaluate probabilistic shaping with time-varying correlations.

(higher effective SNR and smaller  $\eta$ ) has in general a smaller PAPR, smaller 4D kurtosis and smaller variance of the transmitted 4D symbols' energy, which highlights the fact that all these performance metrics are inherently related to NLI. However, PAPR only partially reflects the energy variation of symbols (depends on the few constellation points) and 2D kurtosis  $\Phi_2$  neglects the 4D geometry (only takes the 2D symbol energy into account). From the optimization process shown in Fig. 5, we can see that PAPR and  $\Phi_2$  can not reflect well the trend of modulation-dependent nonlinear tolerance (effective SNR and  $\eta$ ) for dual-polarization transmission systems, and thus cannot reflect the complete nonlinear performance. These two performance metrics can only be regarded as a rough indication of nonlinearity tolerance of the 4D formats. In contrast, Kurtosis of 4D symbols  $\Phi_4$  and the variance of 4D symbol energy  $\Psi$  are able to capture the partial effect of dual-polarizations symbol statistics on the NLI, and thus, they are in general consistent with the trend of effective SNR and NLI power coefficient  $\eta$ , but they are not exactly matching. Therefore, we conjecture that  $\Phi_4$  or  $\Psi$  can be also considered as efficient performance metrics for designing NLI-tolerant 4D modulation formats by avoiding the complex perturbation approach for calculating the average NLI power coefficient  $\eta$ . The coefficient  $\eta$  for DP-4D formats has been derived in [62] and demonstrated to predict the NLI in optical systems in [74].  $\triangle$

We conclude this section by emphasizing that the four examples above showed that adding proper constraints in the optimization can reduce the transceivers complexity and penalty for implementation MD-GS modulation formats. Such constraints could allow us to design higher SE modulation formats and introduce specific correlations between different dimensions as the number of dimension increases. As we will see in the next two sections, optimized 4D modulation formats and its optimized labeling provide an excellent transmission performance with respect to conventional QAM and SP-QAM modulation formats in optical transmission system.

*Remark 1:* All of these existing optimized modulation formats obtained with constraints have not been proven to be the best for either the AWGN channel or the optical fiber channel for the BICM paradigm. Finding the optimum modulation formats remains an open research problem. Despite this cautionary statement, the methods discussed above are known to perform well based on bit-wise decoders in terms of GMI, as shown in Sec. V and Sec. VI.

## V. AWGN-OPTIMIZED 4D GEOMETRIC SHAPING FOR OPTICAL TRANSMISSION

In this section, we evaluate the performance of AWGN-optimized 4D constellations in the fibre-optic channel using SSFM simulations. To target a practical SD-FEC with 20%-25% overhead, the optimizations were performed for the AWGN channel at an SNR for which  $GMI \approx 0.85m$  bit/4D-sym for six different SEs:  $m \in \{5, 6, 7, 8, 9, 10\}$ . The recently proposed 4D modulation format with SE of 6 bit/4D-sym, i.e., 4D-64PRS [34], is chosen for  $m = 6$ . In order to make the modulation more structured and reduce the optimization



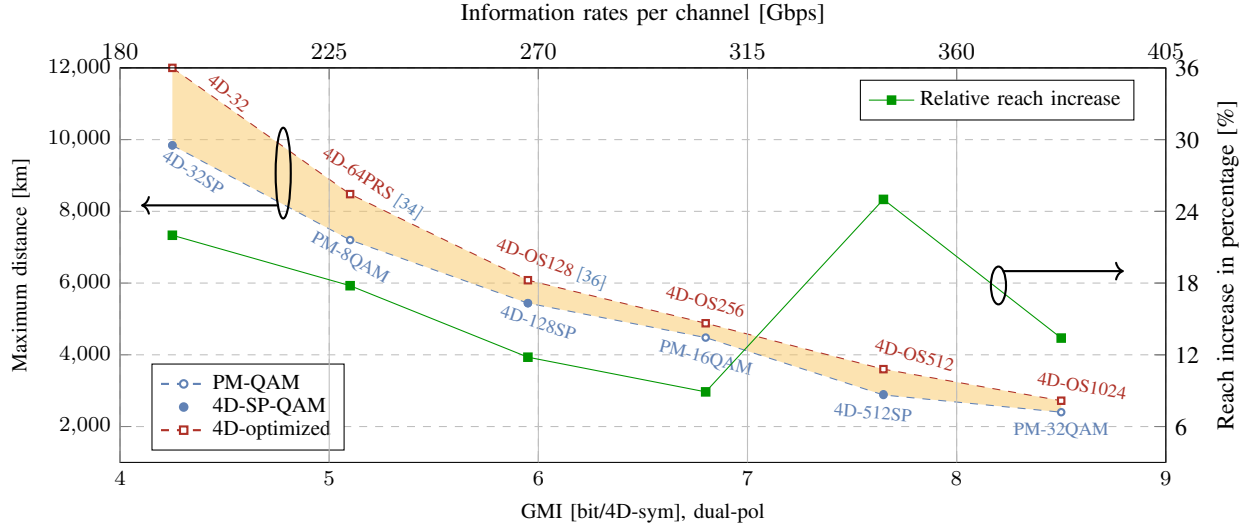


Fig. 6. The maximum reach of various modulation formats for multi-span optical fiber transmission. The markers show the maximum transmission distance at  $\text{GMI} = 0.85m$  for various 4D modulation formats. PM-QAM and 4D SP-QAM are also shown as a reference.

complexity as discussed in Sec. IV, the OS constraint is added for  $m = \{7, 8, 9, 10\}$ . For the transmission system and SD-FEC under consideration, the received SNR varies between 5 dB and 15 dB. Aiming at the target of  $\text{GMI} \approx 0.85m$  bit/4D-sym, we optimize the six modulation formats for a received SNR of 6, 8, 9.5, 10, 11 and 13 dB, respectively. The geometrically-shaped 4D modulation formats with coordinates and labeling are designed by solving Eq. (8) under the AWGN assumption and using a gradient descent algorithm with the end-to-end autoencoder-learning approach in [27].

The optimization process in detail for the geometrically-shaped 4D modulation formats is as follows. At the transmitter, binary vectors are first encoded as an “one-hot” vector as input and are mapped to constellation points via a neural network (NN). We consider a simplified NN with no hidden layers, which only consists of a fully-connected input layer and an output layer. Normalization layer is performed to ensure the power constraint after the output layer. The Gauss–Hermite quadrature is used for computing the GMI as a cost function to remove stochastic effects and the OS constraint is added in the optimization for reducing the complexity. For a special case of all zero biases, the weights directly correspond to the coordinates of the constellation points. These weights can be initialized with random variables or specific values. However, initializing the neural network weights with Gray-labeled QAM is known to be good for BICM systems and can accelerate the learning process compared to a random initialization. Therefore, we use the first orthant of PM-QAM and SP-QAM with Gray-labeling for generating the initial constellations and pre-training the initial weights<sup>3</sup>. The NN parameters are optimized using the Adam optimizer [78] with learning rate 0.01 to obtain the optimized coordinates of the constellation points.

The considered system for evaluating the transmis-

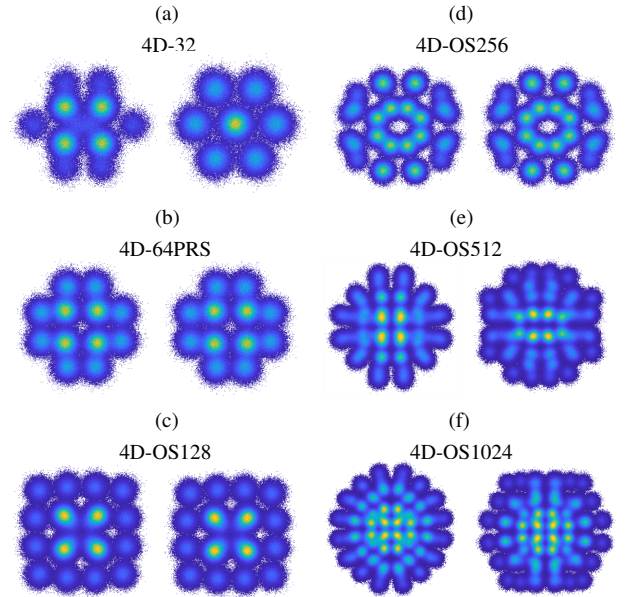


Fig. 7. Constellation diagrams of 4D modulation formats in  $2 \times 2\text{D}$  projection with SEs of 5–10 bit/4D-sym for a received  $\text{GMI} \approx 0.95m$  bit/4D-sym as (a) - (f).

sion performance of the modulation formats is a dual-polarization long-haul WDM transmission system with 11 co-propagating channels over a multi-span of SSMF with attenuation parameter  $\alpha = 0.21$  dB/km, dispersion parameter  $D = 16.9$  ps $\cdot$ nm $^{-1}$ ·km $^{-1}$ , and nonlinear coefficient  $\gamma = 1.31$  W $^{-1}$ ·km $^{-1}$ . Each span consists of an 80 km SSMF through a split-step Fourier solution of the nonlinear Manakov equation with 800 steps per span and is followed by an erbium-doped fiber amplifier (EDFA) with noise figure of 5 dB. Each WDM channel transmits a symbol rate of 45 Gbaud signal with channel spacing of 50 GHz and roll-off factor of 0.1 for root-raised-cosine filter. At the receiver side, the DSP includes electronic chromatic dispersion compensation and matched filtering followed by ideal phase rotation compensation. The performance of the center WDM channel is evaluated.

<sup>3</sup>Due to the limited number of constellation points, the OS constraint is removed for optimizing 5 bit/4D-sym modulation format. The 4D 32-ary Voronoi constellation [77] with an optimized initial labeling is used as the initial constellation.

In Fig. 6, the maximum transmission distance and the relative reach increase in percentage at GMI = 0.85m bit/4D-sym of twelve modulation formats are evaluated. We observe that 4D-optimized formats achieve approximately 320-2160 km (9%-25%) reach increase w.r.t PM-QAM/4D-SP-QAM at the same information rates, which are highlighted by the orange shaded region. We note from Fig. 6 that larger reach increase in percentage can be achieved w.r.t the QAM modulations without gray labeling. Especially comparing to 4D-SP32 and 4D-SP512, the gains of 4D-optimized formats are more than 20%, which is mainly due to the superior performance of labeling.

Fig. 7 shows the optimized 4D modulation formats, i.e., 4D-32, 4D-64PRS and 4D-OSM (here,  $M$  is taken to mean  $M$ -ary constellations), for a received GMI of  $0.95 \times m$  bit/4D-sym.<sup>4</sup> It shows the 4D symbol in each 2D projection, whereas the symbol probability in 2D is proportional to the color brightness via yellow/blue colored heatmap. It can be noticed that all the 4D modulations have symmetric shapes in each 2D, but they are not always X-pol/Y-pol symmetric. Here, X-pol/Y-pol symmetry means that for all the 4D constellation points, if  $[s_i^{1,2}, s_i^{3,4}] \in \mathcal{S}$ ,  $[s_i^{3,4}, s_i^{1,2}]$  must be a valid 4D constellation point in  $\mathcal{S}$ . Interestingly, the asymmetries can especially be specially visible in the higher cardinality configurations, i.e., 4D-OS512 and 4D-OS1024, but also for 4D-32.

## VI. NLI MODEL-AIDED 4D GEOMETRIC SHAPING

As noted in the previous section, all the modulation formats in Fig. 6 are designed for AWGN channel, with the exception of 4D-64PRS, which uses the heuristic idea of constant-modulus constraint to improve the nonlinearity tolerance. NLI model is a key tool to analyze the performance of optical communication systems and enables the design of nonlinear-tolerant modulation formats. This is the objective of this section.

The standard Gaussian noise (GN) model [79]–[81] ignores dependency of nonlinear effects on the modulation format. Other more advanced models such as the enhanced Gaussian noise (EGN) model [82], [83] and NLI noise model [84] allow more accurate analysis of non-conventional modulation formats by abandoning the gaussianity assumption of GN model. However, these models were introduced in PM systems, so they are only valid for PM-2D modulation formats. For the nonlinear fiber channel, 4D NLI model considering modulation-dependent interference for all possible dual polarization four-dimensional (DP-4D) constellations have been proposed in [62] and evaluated in [74], [85]. 4D NLI model could provide a quick computation of the NLI power as a function of the input 4D modulation, which aims at “shaping-out” the 4D modulation-dependent NLI term.

To evaluate the NLI, the effective SNR, which represents the post-DSP SNR at the receiver, is defined as

$$\Gamma \triangleq \frac{P}{\sigma_{\text{ASE}}^2 + \sigma_{\text{NLI}}^2}, \quad (9)$$

<sup>4</sup>The optimized constellation coordinates and bit-to-symbol mappings are available at <https://github.com/TUe-ICTLab/Binary-Labeling-for-2D-and-4D-constellations>.

where  $P$ ,  $\sigma_{\text{ASE}}^2$  and  $\sigma_{\text{NLI}}^2$  represent the transmitted power, the variance of the amplified spontaneous emission noise (ASE) and the NLI variance, respectively.

For general 4D formats, the NLI noise term  $\sigma_{\text{NLI}}^2$  in Eq. (9) can be approximated as two nonidentical NLI powers over the two polarization channels as [62, Eqs. (42) and (43)]

$$\sigma_{\text{NLI}}^2 = \sigma_{\text{NLI,x}}^2 + \sigma_{\text{NLI,y}}^2 = \eta_x(\mathcal{P}, \mathcal{S})P^3 + \eta_y(\mathcal{P}, \mathcal{S})P^3, \quad (10)$$

where  $\eta_x(\cdot)$  and  $\eta_y(\cdot)$  are functions of a given system configuration  $\mathcal{P}$  (fiber link parameters, launch power, etc.) and the 4D modulation format  $\mathcal{S}$ , linked to the contributions of the modulation-dependent nonlinearities in the X- and Y-polarization, respectively. The expression in Eq. (10) includes X-pol and Y-pol interaction effects in the nonlinear terms  $\eta_x$  and  $\eta_y$ , which can be calculated via first-order regular perturbation in [62, Eq. (42)-(43)] and [74, Eq. (1)].<sup>5</sup>

Now that we have defined 4D modulation-dependent NLI and effective SNR, we turn our attention back to the GMI optimization in Eq. (5). Accordingly, to design a nonlinear-tolerant 4D modulation with the effective SNR under consideration, the new optimization problem for a given optical fiber channel parameters  $\mathcal{P}$  can be reformulated as,

$$\{\mathcal{S}^*, \mathcal{B}^*\} = \underset{\mathcal{S}, \mathcal{B}}{\operatorname{argmax}} G(\mathcal{S}, \mathcal{B}, \Gamma_{\text{opt}}), \quad (11)$$

with

$$\Gamma_{\text{opt}} \triangleq \frac{P_{\text{opt}}}{\sigma_{\text{ASE}}^2 + (\eta_x(\mathcal{P}, \mathcal{S}) + \eta_y(\mathcal{P}, \mathcal{S})) P_{\text{opt}}^3}, \quad (12)$$

where  $\Gamma_{\text{opt}}$  denotes the optimum effective SNR for a given system configuration and depends on the modulation format. The optimum value of the launch power is obtained as  $P_{\text{opt}} = \sqrt[3]{\frac{\sigma_{\text{ASE}}^2}{2(\eta_x(\mathcal{P}, \mathcal{S}) + \eta_y(\mathcal{P}, \mathcal{S}))}}$  by setting  $\frac{\partial \Gamma}{\partial P}$  (from Eq. (9)) to zero. Thus, the optimum effective SNR in Eq. (12) can be rewritten as

$$\Gamma_{\text{opt}} = \frac{2}{3\sqrt[3]{2}} \frac{1}{(\sigma_{\text{ASE}}^2)^{2/3} (\eta_x(\mathcal{P}, \mathcal{S}) + \eta_y(\mathcal{P}, \mathcal{S}))^{1/3}}. \quad (13)$$

From the analysis above, we can see that the GMI (see Eq. (11)), is not only dependent on labeled constellation  $\{\mathcal{S}, \mathcal{B}\}$ , but also the NLI noise via  $\Gamma_{\text{opt}}$  in Eq. (13). Note that for a fixed parameter  $\mathcal{P}$ , the modulation-dependent NLI noise is also a function of  $\mathcal{S}$ . Thus, the introduced NLI model-aided geometric shaping is actually only dependent on the shape of modulation formats and without the need of SNR or power optimization, which is equivalent to add a constraint and reduce the dimensionality of the optimization space.

We consider a dual-polarized, single channel waveform over a single span of SSMF. The same fiber parameters (including dispersion, attenuation and nonlinearity) as in Sec. V are used for both 4D NLI model and SSFM simulation. We solve Eq. (11) by adding the OS constraint and also using the end-to-end AE-learning method described before. The 4D NLI model can be considered as a surrogate channel in the end-

<sup>5</sup>Note that in this paper, only signal-signal nonlinear interactions are considered along the fibre propagation in  $\sigma_{\text{NLI}}^2$ . For a more accurate NLI estimation, signal-noise NLI interaction with 4D-modulation dependent contributions should be also considered, e.g., as done in [85].

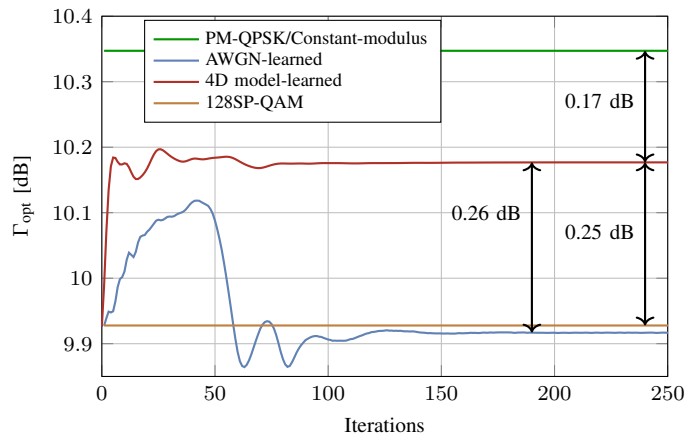


Fig. 8. The optimum effective SNR  $\Gamma_{\text{opt}}$  versus the number of optimization iteration at 234 km of geometrically shaped 4D 128-ary modulation format optimized based on AWGN channel and 4D NLI model.

to-end learning structure, thus, gradient descent needs to be applied to constellation coordinates and optimum effective SNR both for maximizing GMI. Similar 4D NLI model-aided 4D modulation optimization has been also done in [40], however lifting any geometrical constraint and targeting only symbol-wise coded modulation systems by maximizing MI for a multi-span transmission scenario.

In Fig. 8 and Fig. 9, the optimum effective SNR and GMI trace as a function of the optimization steps are shown for the optimization procedure. The 4D modulation formats with a SE of 7 bit/4D-sym are optimized with OS constraint via end-to-end learning following [27] by maximizing GMI. The simulations are implemented by solving two optimization problems with similar effective SNRs around 10 dB: one is for the AWGN channel with SNR=10 dB (AWGN-learned) and the other is for 4D NLI-model [62] with a single-channel, 234 km single-span transmission system (4D model-learned). PM-QPSK as a format with a good nonlinearity tolerance and 4D-128SP-QAM [55] with 7 bit/4D-sym are shown as references.

Fig. 8 shows that the 4D model-learned modulation can tolerate higher nonlinearities. This can be seen from the achieved 0.25 dB gain with respect to 128SP-QAM and AWGN-learned 4D modulation in terms of  $\text{SNR}_{\text{opt}}$  at 234 km. In contrast, PM-QPSK or 4D constant-modulus modulation formats show that a potential effective SNR gain of 0.42 dB for nonlinearity tolerance could be provided. The 4D model-learned modulation achieves more than half of this gain, which is translated into a GMI increase as explained below.

Fig. 9 shows that in an AWGN channel with an SNR of 10 dB (dashed curves), both AWGN-learned modulation format and 4D model-learned modulation format outperform 128SP-QAM with a gain of 0.22 bit/4D and 0.18 bit/4D, respectively. However, by considering an optical fiber channel with length of 234 km (solid curves), the gain of the 4D model-learned modulation is increased to 0.29 bit/4D compared to 128SP-16QAM, which is higher than that of the AWGN-learned format. These benefits (approximately 0.11 bit/4D GMI gain) come from the improvement of  $\text{SNR}_{\text{opt}}$  shown in Fig. 8 due to its excellent nonlinear-tolerant property. The

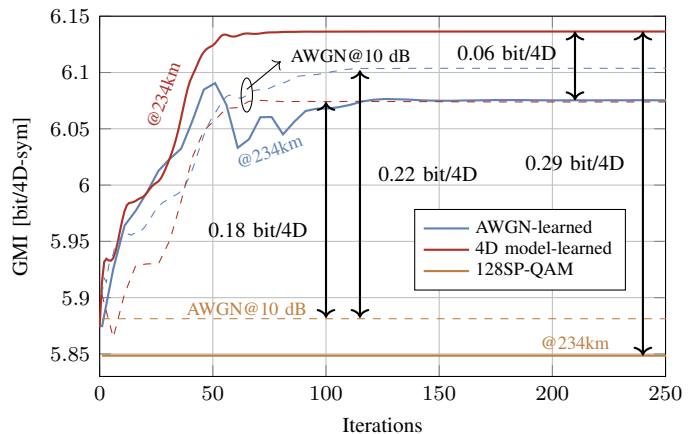


Fig. 9. GMI versus the number of optimization iteration at 234 km of geometrically shaped 4D 128-ary modulation format optimized based on AWGN channel and 4D NLI model.

relative additional shaping gain in terms of GMI for the nonlinear channel with respect to the gain in the linear channel is  $(0.29 - 0.18)/0.18 = 38\%$ . It well-matched to the fact that 4D model-learned modulations lead to a good trade-off between linear and nonlinear shaping gain by increasing the linear shaping gain and maintaining a fair level of nonlinearity tolerance.

In Fig. 10, we show the effective SNR and GMI performance of three modulation formats through a split-step Fourier solution of the nonlinear Manakov equation. We can observe that the 4D model-learned modulation outperforms both 128SP-QAM and AWGN-learned 4D modulation in term of effective SNR and GMI, which is close to the observed gain in 4D NLI model prediction in Fig. 8 and Fig. 9. Normally, a GS modulation format will lead to a larger SNR penalty. However, the 4D model-learned modulation format provides a larger effective SNR (0.25 dB gain) compared to 128SP-16QAM at the optimal launch power in Fig. 10 (a), which is consistent with the analysis in Sec. II-C. In addition, both the AWGN-learned format and 128SP-QAM lead to a larger effective SNR degradation than 4D model-learned modulation format in nonlinear region (high launch power). Therefore, the shaping gain in the linear region can be increased in nonlinear region and translates into a larger reach increase. In Fig. 10 (b), we can also observe that the GMI gain of AWGN-learned modulation over 4D model-learned modulation in linear region is vanished in nonlinear region.

Fig. 10 (c) shows GMI as a function of transmission distance for three different modulation formats using the optimal launch power at each distance. The received symbols in 2D projection (X-pol/Y-pol) of the 4D model-learned modulation is plotted in the inset of Fig. 10 (c). We can observe that the proposed 4D model-learned modulation format leads to a 4 km (2%) increase in reach relative to the 128SP-16QAM modulation format at GMI of 6.1 bit/4D-sym. In addition, 4D model-learned format performs better than AWGN-learned format with a gain of about 1 km in all the distances between 220 km and 240 km.

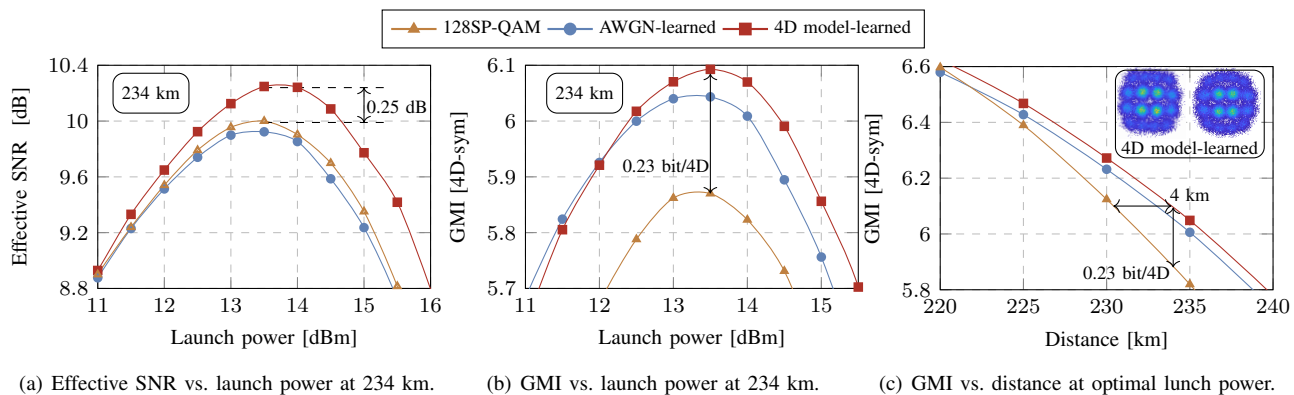


Fig. 10. Simulation results of single-span optical fiber transmission with single channel for three modulation formats: 128SP-QAM, AWGN-learned 4D modulation and 4D model-learned modulation.

## VII. CONCLUSIONS

In this paper, we reviewed the existing multi-dimensional geometrically-shaped modulation formats for fiber optical communication systems and showed that they could provide potentially larger gains. The key challenges and different methods for overcoming the limitations associated with the develop of MD-GS formats were presented and discussed. The main focus of this paper was on the 4D modulation formats for dual-polarization optical fiber channel. With the aid of adding efficient constraints for optimizing modulation formats, we numerically assessed a series of 4D modulation formats via numerical simulation. We showed that the 4D-optimized modulation formats can be a solution for multi-rate applications between 5 and 10 bit/dual-pol with a transmission reach extension of up to 25% in multi-span systems. In addition, up to 0.25 dB NLI gains in terms of effective SNR are demonstrated for NLI model-optimized modulation over regular 4D format and Gaussian channel-optimal 4D format in a single-span transmission system. The results in this work confirm that the multi-dimensional modulations could be a good alternative for high capacity transmission systems and offer substantial potential gains in the nonlinear optical fiber channel.

Note that the performance of MD modulation also depends on which dimensions are selected. The methods described in this paper can be extended to nonlinear optical channel by jointly combing other dimensions with different correlated property and also to channels with memory. This is left for further investigation.

All the analysis presented in this paper was only considered bitwise decoder (i.e., BICM) for multi-dimensional geometric shaping. Better performance are expected if a hybrid CM with combing of BICM and multi-stage decoding are used. In these cases, we conjecture the a performance metric of combing MI and GMI to be the correct metric to design MD modulation formats. This investigation and comparison are interesting future research avenues.

## REFERENCES

- [1] B. Chen, G. Liga, Y. Lei, W. Ling, Z. Huan, X. Xue, and A. Alvarado, "Shaped four-dimensional modulation formats for optical fiber communication systems," in *Opt. Fiber Commun. Conf. (OFC)*, Mar. 2022.
- [2] G. Ungerboeck, "Channel coding with multilevel/phase signals," *IEEE Trans. Inf. Theory*, vol. 28, no. 1, pp. 55–67, Jan. 1982.
- [3] "Nokia PSE-V technical white paper." [Online]. Available: <https://onestore.nokia.com/asset/207220>
- [4] "1FINITY T600 transport blade." [Online]. Available: <https://www.fujitsu.com/us/Images/1FINITY-T600-Data-Sheet.pdf>
- [5] L. Szczecinski and A. Alvarado, *Bit-interleaved coded modulation: fundamentals, analysis and design*. John Wiley & Sons, 2015.
- [6] F. Steiner and G. Böcherer, "Comparison of geometric and probabilistic shaping with application to ATSC 3.0," in *11th International ITG Conference on Systems, Communications and Coding (SCC)*, Feb. 2017.
- [7] E. Sillekens, D. Semrau, D. Lavery, P. Bayvel, and R. I. Killey, "Experimental demonstration of geometrically-shaped constellations tailored to the nonlinear fibre channel," in *2018 Eur. Conf. on Opt. Commun. (ECOC)*, Sep. 2018.
- [8] H. Dzieciol, G. Liga, E. Sillekens, P. Bayvel, and D. Lavery, "Geometric shaping of 2-D constellations in the presence of laser phase noise," *J. Lightw. Technol.*, vol. 39, no. 2, pp. 481–490, Jan. 2021.
- [9] G. Welti and J. Lee, "Digital transmission with coherent four-dimensional modulation," *IEEE Trans. Inf. Theory*, vol. 20, no. 4, pp. 497–502, Jul. 1974.
- [10] G. Foschini, R. Gitlin, and S. Weinstein, "Optimization of two-dimensional signal constellations in the presence of gaussian noise," *IEEE Trans. on Commun.*, vol. 22, no. 1, pp. 28–38, Jan. 1974.
- [11] L. Zetterberg and H. Brandstrom, "Codes for combined phase and amplitude modulated signals in a four-dimensional space," *IEEE Trans. on Commun.*, vol. 25, no. 9, pp. 943–950, Sep. 1977.
- [12] T. H. Lotz, X. Liu, S. Chandrasekhar, P. J. Winzer, H. Haunstein, S. Randel, S. Corteselli, B. Zhu, and D. W. Peckham, "Coded PDM-OFDM transmission with shaped 256-iterative-polar-modulation achieving 11.15-b/s/Hz intrachannel spectral efficiency and 800 km reach," *J. Lightw. Technol.*, vol. 31, no. 4, pp. 538–545, Feb. 2013.
- [13] S. Zhang, F. Yaman, E. Mateo, T. Inoue, K. Nakamura, and Y. Inada, "Design and performance evaluation of a GMI-optimized 32QAM," in *2017 Eur. Conf. on Opt. Commun. (ECOC)*, Sep. 2017.
- [14] B. Chen, C. Okonkwo, H. Hafermann, and A. Alvarado, "Increasing achievable information rates via geometric shaping," in *2018 Eur. Conf. on Opt. Commun. (ECOC)*, Sep. 2018.
- [15] B. Chen, C. Okonkwo, D. Lavery, and A. Alvarado, "Geometrically-shaped 64-point constellations via achievable information rates," in *20th Int. Conf. on Transparent Opt. Netw. (ICTON)*, Jul. 2018.
- [16] R. T. Jones, T. A. Eriksson, M. P. Yankov, and D. Zibar, "Deep learning of geometric constellation shaping including fiber nonlinearities," in *2018 Eur. Conf. on Opt. Commun. (ECOC)*, Sep. 2018.
- [17] S. Li, C. Häger, N. Garcia, and H. Wymeersch, "Achievable information rates for nonlinear fiber communication via end-to-end autoencoder learning," in *Eur. Conf. on Opt. Commun. (ECOC)*, Sep. 2018.
- [18] M. Schaedler, S. Calabrò, F. Pittalà, G. Böcherer, M. Kuschnerov, C. Bluemm, and S. Pachnicke, "Neural network assisted geometric shaping for 800 Gbit/s and 1 Tbit/s optical transmission," in *Opt. Fiber Commun. Conf. (OFC)*, Mar. 2020.
- [19] R. T. Jones, M. P. Yankov, and D. Zibar, "End-to-end learning for GMI optimized geometric constellation shape," in *Eur. Conf. Opt. Commun. (ECOC)*, Sep. 2019.
- [20] A. Soleimanzade and M. Ardakani, "EGN-based optimization of the APSK constellations for the non-linear fiber channel based on the symbol-wise mutual information," *J. Lightw. Technol.*, vol. 40, no. 7, pp. 1937–1952, Apr. 2022.

- [21] O. Jovanovic, M. P. Yankov, F. D. Ros, and D. Zibar, "End-to-end learning of a constellation shape robust to variations in SNR and laser linewidth," in *Eur. Conf. Opt. Commun. (ECOC)*, Jun. 2021.
- [22] A. Rode, B. Geiger, and L. Schmalen, "Geometric constellation shaping for phase-noise channels using a differentiable blind phase search," in *Opt. Fiber Commun. Conf. (OFC)*, Mar. 2022.
- [23] L. Galdino, A. Edwards, W. Yi, E. Sillekens, Y. Wakayama, T. Gerard, W. S. Pelouch, S. Barnes, T. Tsuritani, R. I. Killey, D. Lavery, and P. Bayvel, "Optical fibre capacity optimisation via continuous bandwidth amplification and geometric shaping," *IEEE Photon. Technol. Lett.*, vol. 32, no. 17, pp. 1021–1024, Sep. 2020.
- [24] M. Ionescu, D. Lavery, A. Edwards, E. Sillekens, D. Semrau, L. Galdino, R. I. Killey, W. Pelouch, S. Barnes, and P. Bayvel, "74.38 Tb/s transmission over 6300 km single mode fibre enabled by C+L amplification and geometrically shaped PDM-64QAM," *J. Lightw. Technol.*, vol. 38, no. 2, pp. 531–537, Mar. 2020.
- [25] G. Forney, R. Gallager, G. Lang, F. Longstaff, and S. Qureshi, "Efficient modulation for band-limited channels," *IEEE Journal on Selected Areas in Communications*, vol. 2, no. 5, pp. 632–647, Sep. 1984.
- [26] L. Beygi, E. Agrell, J. M. Kahn, and M. Karlsson, "Coded modulation for fiber-optic networks: Toward better tradeoff between signal processing complexity and optical transparent reach," *IEEE Signal Processing Magazine*, vol. 31, no. 2, pp. 93–103, Mar. 2014.
- [27] K. Gümüř, A. Alvarado, B. Chen, C. Häger, and E. Agrell, "End-to-end learning of geometrical shaping maximizing generalized mutual information," in *Opt. Fiber Commun. Conf. (OFC)*, Mar. 2020.
- [28] E. Sillekens, G. Liga, D. Lavery, P. Bayvel, and R. I. Killey, "High-cardinality geometrical constellation shaping for the nonlinear fiber channel," *arXiv e-prints*, May 2022. [Online]. Available: <https://arxiv.org/abs/2205.04391>
- [29] M. Karlsson and E. Agrell, "Which is the most power-efficient modulation format in optical links?" *Opt. Express*, vol. 17, no. 13, pp. 10814–10819, Jun. 2009.
- [30] E. Agrell and M. Karlsson, "Power-efficient modulation formats in coherent transmission systems," *J. Lightw. Technol.*, vol. 27, no. 22, pp. 5115–5126, Nov. 2009.
- [31] M. Chagnon, M. Osman, Q. Zhuge, X. Xu, and D. V. Plant, "Analysis and experimental demonstration of novel 8PolSK-QPSK modulation at 5 bits/symbol for passive mitigation of nonlinear impairments," *Opt. Express*, vol. 21, no. 25, pp. 30204–30220, Dec. 2013.
- [32] T. Nakamura, E. L. T. de Gabory, H. Noguchi, W. Maeda, J. Abe, and K. Fukuchi, "Long haul transmission of four-dimensional 64SP-12QAM signal based on 16QAM constellation for longer distance at same spectral efficiency as PM-8QAM," in *2015 Eur. Conf. on Opt. Commun. (ECOC)*, Sep. 2015.
- [33] K. Kojima, T. Yoshida, T. Koike-Akino, D. S. Millar, K. Parsons, M. Pajovic, and V. Arlunno, "Nonlinearity-tolerant four-dimensional 2A8PSK family for 5-7 bits/symbol spectral efficiency," *J. Lightw. Technol.*, vol. 35, no. 8, pp. 1383–1391, Apr. 2017.
- [34] B. Chen, C. Okonkwo, H. Hafermann, and A. Alvarado, "Polarization-ring-switching for nonlinearity-tolerant geometrically-shaped four-dimensional formats maximizing generalized mutual information," *J. Lightw. Technol.*, vol. 37, no. 14, pp. 3579–3591, Jul. 2019.
- [35] S. van der Heide, B. Chen, M. van den Hout, G. Liga, T. Koonen, H. Hafermann, A. Alvarado, and C. Okonkwo, "11,700 km transmission at 4.8 bit/4D-sym via four-dimensional geometrically-shaped polarization-ring-switching modulation," in *Opto-Electron. and Commun. Conf. (OECC) and Int. Conf. on Photon. in Switch. and Comput. (PSC)*, Jul. 2019.
- [36] B. Chen, A. Alvarado, S. van der Heide, M. van den Hout, H. Hafermann, and C. Okonkwo, "Analysis and experimental demonstration of orthant-symmetric four-dimensional 7 bit/4D-sym modulation for optical fiber communication," *J. Lightw. Technol.*, vol. 39, no. 9, pp. 2737–2753, May. 2021.
- [37] S. Goossens, Y. C. Gültekin, O. Vassilieva, P. P. Inwoong Kim, C. Okonkwo, and A. Alvarado, "4D geometric shell shaping with applications to 400ZR," *arXiv e-prints*, Jun. 2022. [Online]. Available: <https://arxiv.org/abs/2206.03251>
- [38] S. Goossens, Y. C. Gültekin, O. Vassilieva, I. Kim, P. Palacharla, C. Okonkwo, and A. Alvarado, "Introducing 4D geometric shell shaping," *arXiv e-prints*, Jun. 2022. [Online]. Available: <https://arxiv.org/abs/2206.03341>
- [39] F. Frey, S. Stern, J. K. Fischer, and R. Fischer, "Two-stage coded modulation for Hurwitz constellations in fiber-optical communications," *J. Lightw. Technol.*, vol. 38, no. 12, pp. 3135–3146, Jun. 2020.
- [40] G. Liga, B. Chen, and A. Alvarado, "Model-aided geometrical shaping of dual-polarization 4D formats in the nonlinear fiber channel," in *Opt. Fiber Commun. Conf. (OFC)*, Mar. 2022.
- [41] A. D. Shiner, M. Reimer, A. Borowiec, S. O. Gharan, J. Gaudette, P. Mehta, D. Charlton, K. Roberts, and M. O'Sullivan, "Demonstration of an 8-dimensional modulation format with reduced inter-channel nonlinearities in a polarization multiplexed coherent system," *Opt. Express*, vol. 22, no. 17, pp. 20366–20374, Aug. 2014.
- [42] D. F. Bendimerad, H. Hafermann, and H. Zhang, "Nonlinearity-tolerant 8D modulation formats by set-partitioning PDM-QPSK," in *2018 Opt. Fiber Commun. Conf. (OFC)*, Mar. 2018.
- [43] A. I. Abd El-Rahman and J. C. Cartledge, "Evaluating the impact of QAM constellation subset selection on the achievable information rates of multidimensional formats in fully loaded systems," *J. Lightw. Technol.*, vol. 36, no. 3, pp. 712–720, Feb. 2018.
- [44] T. Koike-Akino, D. S. Millar, K. Kojima, and K. Parsons, "Eight-dimensional modulation for coherent optical communications," in *Eur. Conf. on Opt. Commun. (ECOC)*, Sep. 2013.
- [45] B. Chen, C. Okonkwo, H. Hafermann, and A. Alvarado, "Eight-dimensional polarization-ring-switching modulation formats," *IEEE Photon. Technol. Lett.*, vol. 31, no. 21, pp. 1717–1720, Nov. 2019.
- [46] S. van der Heide, B. Chen, M. van den Hout, H. Hafermann, T. Koonen, A. Alvarado, and C. Okonkwo, "Experimental demonstration of eight-dimensional modulation formats for long-haul optical transmission," in *Eur. Conf. Opt. Commun. (ECOC)*, Sep. 2019.
- [47] R.-J. Essiambre, R. Ryf, S. v. der Heide, J. I. Bonetti, H. Huang, M. Kodialam, F. J. García-Gómez, E. C. Burrows, J. C. Alvarado-Zacarias, R. Amezcua-Correa, X. Chen, N. K. Fontaine, and H. Chen, "First transmission of a 12D format across three coupled spatial modes of a 3-core coupled-core fiber at 4 bits/s/Hz," in *Opt. Fiber Commun. Conf. (OFC)*, Mar. 2020.
- [48] G. Rademacher, B. J. Puttnam, R. S. Luís, Y. Awaji, N. Wada, E. Agrell, and K. Petermann, "Experimental investigation of a 16-dimensional modulation format for long-haul multi-core fiber transmission," in *Eur. Conf. Opt. Commun. (ECOC)*, Sep. 2015.
- [49] D. S. Millar, T. Koike-Akino, K. Kojima, and K. Parsons, "A 24-dimensional modulation format achieving 6 dB asymptotic power efficiency," in *Advanced Photonics 2013*, Jul. 2013.
- [50] D. S. Millar, T. Koike-Akino, R. Maher, D. Lavery, M. Paskov, K. Kojima, K. Parsons, B. C. Thomsen, S. J. Savory, and P. Bayvel, "Experimental demonstration of 24-dimensional extended Golay coded modulation with LDPC," in *Opt. Fiber Commun. Conf. (OFC)*, Mar. 2014.
- [51] D. S. Millar, T. Koike-Akino, S. Ö. Arık, K. Kojima, K. Parsons, T. Yoshida, and T. Sugihara, "High-dimensional modulation for coherent optical communications systems," *Opt. Express*, vol. 22, no. 7, pp. 8798–8812, Apr. 2014.
- [52] A. Mirani, E. Agrell, and M. Karlsson, "Low-complexity geometric shaping," *J. Lightw. Technol.*, vol. 39, no. 2, pp. 363–371, Jan. 2021.
- [53] R. Rios-Müller, J. Renaudier, O. Bertran-Pardo, A. Ghazisaeidi, P. Tran, G. Charlet, and S. Bigo, "Experimental comparison between hybrid-QPSK/8QAM and 4D-32SP-16QAM formats at 31.2 GBaud using Nyquist pulse shaping," in *Eur. Conf. on Opt. Commun. (ECOC)*, Sep. 2013.
- [54] H. Sun, R. Egorov, B. E. Basch, J. McNicol, and K. Wu, "Comparison of two modulation formats at spectral efficiency of 5 bits/dual-pol symbol," in *Eur. Conf. on Opt. Commun. (ECOC)*, Sep. 2013.
- [55] T. A. Eriksson, M. Sjödin, P. Johannisson, P. A. Andrekson, and M. Karlsson, "Comparison of 128-SP-QAM and PM-16QAM in long-haul WDM transmission," *Opt. Express*, vol. 21, no. 16, pp. 19269–19279, Aug. 2013.
- [56] A. S. Kashi, J. C. Cartledge, A. Bakhshali, A. Rezaei, A. I. A. El-Rahman, M. O'Sullivan, C. Laperle, A. Borowiec, and K. Roberts, "Information rates for the SP 128-QAM and DP 16-QAM modulation formats," in *2015 Eur. Conf. on Opt. Commun. (ECOC)*, Sep. 2015.
- [57] K. Wang, J. Yu, P. Gou, M. Zhao, K. Lyu, and X. Xin, "Transmission performance comparison of 128-SP-QAM and PM-16QAM in a WDM system," *Optical Fiber Technology*, vol. 43, pp. 158–162, May 2018.
- [58] R. Dar, M. Feder, A. Mecozzi, and M. Shtaif, "On shaping gain in the nonlinear fiber-optic channel," in *IEEE Int. Symp. on Inf. Theory*, Jun. 2014.
- [59] M. Reimer, S. O. Gharan, A. D. Shiner, and M. O'Sullivan, "Optimized 4 and 8 dimensional modulation formats for variable capacity in optical networks," in *2016 Opt. Fiber Commun. Conf. (OFC)*, Mar. 2016.
- [60] R.-J. Essiambre, R. Ryf, M. Kodialam, B. Chen, M. Mazur, J. I. Bonetti, R. Veronese, H. Huang, A. Gupta, F. A. Aoudia, E. C. Burrows, D. F. Grosz, L. Palmieri, M. Sellathurai, X. Chen, N. K. Fontaine, and H. Chen, "Increased reach of long-haul transmission using a constant-power 4D format designed using neural networks," in *Eur. Conf. Opt. Commun. (ECOC)*, Dec. 2020.

- [61] T. A. Eriksson, P. Johannisson, M. Sjödin, E. Agrell, P. A. Andrekson, and M. Karlsson, "Frequency and polarization switched QPSK," in *Eur. Conf. Opt. Commun. (ECOC)*, Sep. 2013.
- [62] G. Liga, A. Barreiro, H. Rabbani, and A. Alvarado, "Extending fibre nonlinear interference power modelling to account for general dual-polarisation 4D modulation formats," *Entropy*, vol. 22, no. 11, pp. 1–38, Nov. 2020.
- [63] B. P. Smith and F. R. Kschischang, "A pragmatic coded modulation scheme for high-spectral-efficiency fiber-optic communications," *J. Lightw. Technol.*, vol. 30, no. 13, pp. 2047–2053, Jul. 2012.
- [64] A. Alvarado, T. Fehenberger, B. Chen, and F. M. J. Willems, "Achievable information rates for fiber optics: Applications and computations," *J. Lightw. Technol.*, vol. 36, no. 2, pp. 424–439, Jan. 2018.
- [65] A. Alvarado, E. Agrell, and F. Brännström, "Asymptotic comparison of ML and MAP detectors for multidimensional constellations," *IEEE Trans. Inf. Theory*, vol. 64, pp. 1231–1240, Feb. 2018.
- [66] M. Anedda, A. Meloni, and M. Murrioni, "64-APSK constellation and mapping optimization for satellite broadcasting using genetic algorithms," *IEEE Trans. on Broadcasting*, vol. 62, no. 1, pp. 1–9, Mar. 2016.
- [67] J. Song, C. Häger, J. Schröder, A. G. I. Amat, and H. Wymeersch, "Model-based end-to-end learning for WDM systems with transceiver hardware impairments," *IEEE Journal of Selected Topics in Quantum Electronics*, vol. 28, no. 4, pp. 1–14, Aug. 2022.
- [68] J. Cho and P. J. Winzer, "Probabilistic constellation shaping for optical fiber communications," *J. Lightw. Technol.*, vol. 37, no. 6, pp. 1590–1607, Mar. 2019.
- [69] A. Alvarado and E. Agrell, "Four-dimensional coded modulation with bit-wise decoders for future optical communications," *J. Lightw. Technol.*, vol. 33, no. 10, pp. 1993–2003, May 2015.
- [70] T. Pfau, S. Hoffmann, and R. Noe, "Hardware-efficient coherent digital receiver concept with feedforward carrier recovery for  $m$ -QAM constellations," *J. Lightw. Technol.*, vol. 27, no. 8, pp. 989–999, Apr. 2009.
- [71] S. Almonacil, F. Boitier, and P. Layec, "Performance model and design rules for optical systems employing low-resolution DAC/ADC," *J. Lightw. Technol.*, vol. 38, no. 11, pp. 3007–3014, Jun. 2020.
- [72] S. Li, A. Mirani, M. Karlsson, and E. Agrell, "Low-complexity Voronoi shaping for the Gaussian channel," *IEEE Transactions on Communications*, vol. 70, no. 2, pp. 865–873, Feb. 2022.
- [73] W. Ling, B. Chen, and Y. Lei, "Orthant-symmetric multi-dimensional geometrically-shaped modulation optimization," in *19th Int. Conf. on Optical Commun. and Netw. (ICOCN)*, Aug. 2021.
- [74] G. Liga, B. Chen, A. Barreiro, and A. Alvarado, "Modeling of nonlinear interference power for dual-polarization 4D formats," in *Opt. Fiber Commun. Conf. (OFC)*, Mar. 2021.
- [75] K. Wu, G. Liga, A. Sheikh, F. M. J. Willems, and A. Alvarado, "Temporal energy analysis of symbol sequences for fiber nonlinear interference modelling via energy dispersion index," *J. Lightw. Technol.*, vol. 39, no. 18, pp. 5766–5782, Sep. 2021.
- [76] J. Cho and R. Tkach, "On the kurtosis of modulation formats for characterizing the nonlinear fiber propagation," *J. Lightw. Technol.*, vol. 40, no. 12, pp. 3739–3748, Jun. 2022.
- [77] G. Forney, "Multidimensional constellations. II. Voronoi constellations," *IEEE Journal on Selected Areas in Communications*, vol. 7, no. 6, pp. 941–958, 1989.
- [78] D. P. Kingma and J. Ba, "Adam: A method for stochastic optimization," in *Proc. ICLR*, Dec. 2014.
- [79] P. Poggiolini, G. Bosco, A. Carena, V. Curri, Y. Jiang, and F. Forghieri, "The GN-model of fiber non-linear propagation and its applications," *J. Lightw. Technol.*, vol. 32, no. 4, pp. 694–721, Feb. 2014.
- [80] P. Serena and A. Bononi, "An alternative approach to the Gaussian noise model and its system implications," *J. Lightw. Technol.*, vol. 31, no. 22, pp. 3489–3499, Nov. 2013.
- [81] P. Johannisson and M. Karlsson, "Perturbation analysis of nonlinear propagation in a strongly dispersive optical communication system," *J. Lightw. Technol.*, vol. 31, no. 8, pp. 1273–1282, Apr. 2013.
- [82] A. Carena, G. Bosco, V. Curri, Y. Jiang, P. Poggiolini, and F. Forghieri, "EGN model of non-linear fiber propagation," *Opt. Express*, vol. 22, no. 13, pp. 16 335–16 362, Jun. 2014.
- [83] R. Dar, M. Feder, A. Mecozzi, and M. Shtaif, "Properties of nonlinear noise in long dispersion-uncompensated fiber links," *Opt. Express*, vol. 21, no. 22, pp. 25 685–25 699, Nov. 2013.
- [84] —, "Accumulation of nonlinear interference noise in fiber-optic systems," *Opt. Express*, vol. 22, no. 12, pp. 14 199–14 211, Jun. 2014.
- [85] Z. Liang, B. Chen, Y. Lei, G. Liga, and A. Alvarado, "Extension and validation of 4D model for improving the accuracy of modulation-dependent nonlinear interference," *arXiv e-prints*, Jun. 2022. [Online]. Available: <http://arxiv.org/abs/2206.00866>